Effect of aspect ratio on the Double-diffusive convection of a fluid contained in a rectangular cavity with partially thermally active side walls.

Rasoul Nikbakhti and Asghar Baradaran Rahimi.

Department of Mechanical Engineering, Ferdowsi University of Mashhad

e-mail: rasoul_nikbakhti@yahoo.com

Department of Mechanical Engineering, Ferdowsi University of Mashhad

e-mail: rahimiab@yahoo.com

Abstract. *A numerical study is performed to investigate the effect of height-to-width aspect ratio, Grashof number, and Schmidt number on the Double-diffusive convection of a fluid contained in a rectangular cavity with partially thermally active side walls. The active part of the left side wall is at a higher temperature and concentration than that of the right side wall. The length of the thermally active part is equal to half of the height. The top and bottom of the cavity and inactive part of the side walls are considered to be adiabatic and impermeable to mass transfer. Nine different relative positions of the active zones are considered. The species diffusivity of the fluid is assumed to be constant but the density of fluid is assumed to vary linearly with temperature and concentration. The non-dimensional forms of governing transport equations that describe double-diffusive convection for laminar two-dimensional incompressible flow are functions of vorticity, temperature or energy, concentration and stream-function.*
The coupled differential equations are discretized by the Finite Difference Method. The Successive- Over-Relaxation (SOR) method is used in the solution of the stream function equation. The results are obtained for Grashof numbers between 10^3 *and* 10^6*, The Prandtl number of 0.71, the Schmidt number in the range of* [1, 2], *and the effects of the aspect ratio on the flow, temperature and concentration fields and the rate of heat and mass transfer from the walls of the enclosure are presented. The density inversion of the fluid has a great influence on the natural convection. The heat and mass transfer rate is high for the bottom-top thermally active location while the heat and mass transfer rate is poor in the top-bottom thermally active location. The heat and mass transfer rate is found to be increased with an increase in the aspect ratio and Grashof number.*

Key words: Double diffusive convection, Partially active walls, Aspect ratios, Rectangular cavity, Heat and mass transfer

1. Introduction

During the past 50 years many experimental and numerical studies have been carried out concerning convective phenomena within cells. Most of these studies deal with fluid motion due only to temperature gradients. Nevertheless, fluid motion may be induced by density variations due to gradients of other scalar quantities. One of these quantities can be pollutant concentration within the fluid. Such a phenomenon, combining temperature and concentration buoyancy forces, is called double-diffusion.

Double-diffusion occurs in a very wide range of fields such as oceanography, astrophysics, geology, biology, chemical processes, as well as in many engineering applications such as solar ponds, natural gas storage tanks, crystal manufacturing, and metal solidification processes. Unique double diffusive convection phenomena, such as salt fingers and diffusive interfaces have been observed due to the significant difference in diffusivities of heat and mass [1].

There are many convection modes depending on the directions of temperature and concentration gradients relative to gravity, as pointed out by Ostrach [2].Most of the initial theoretical studies on double diffusive convection have been performed for vertical temperature and concentration gradients for ocean applications using linear stability theory [l].Gebhart and Pera [3] were among the first ones to numerically study double- diffusion for cases of vertical laminar fluid motions along surfaces or in plumes. In this study, special attention was paid to the influence of non-dimensional parameters relevant to double-diffusion, on the heat and mass transport processes ; transition to turbulence was mentioned.In1985, Bejan [4] completed a fundamental study of scale analysis relative to heat and mass transport processes within cavities, submitted to horizontal temperature and concentration gradients. Pure thermal convection, pure solutal convection, heat transfer driven flows, and mass transfer driven flows were taken into account. Furthermore, in another report, Trevisan and Bejan [5] studied the boundary layer flow in the same configuration (under the stationary regime) and varied several non-dimensional parameters: the Lewis and Prandtl numbers, and the buoyancy ratio. Lin et al. [6] repeated a similar study relative to the behaviour of the whole flow, under the unstationary regime. Other numerical works which are mainly concerned with chemical vapour deposition processes [7] dealt with very low Prandtl number (0.01) gases. Beckermann and Viskanta [8] simulated double diffusive layers occurring in a solidification process when a horizontal temperature gradient is present. Considerable discrepancies between numerical solutions and experimental measurements were reported because of the complicated solidification process, which involves phase changes and non-stationary irregular interfaces. When horizontal temperature and concentration gradients are present in a simple rectangular enclosure, steady-state solutions were obtained by Hu and El-Wakil [9] and more recently by Benard et al. [10].Wang et al. [11] and Kamotanier al. [12] initiated preliminary experiments in a rectangular cavity of aspect ratio 0.55. They used an electrochemical system in a copper sulfate-acid solution to simulate the horizontal concentration gradient. The experiments revealed a three-layered flow structure in the core for a certain range of buoyancy ratio. These experimental endeavors were, however, highly restrictive in nature. The above experiments were limited to the early stages of convection, and they were unable to perform the experiments leading to the steady- state.

Lee et al. [13] and Lee and Hyun[14] devised improved experimental techniques by installing vertical membrane walls; exterior to these membranes, solutions of constant preset concentration and temperature were forced to circulate. In this manner, Lee er al. [13] and Lee and Hyun [14] achieved a closer experimental approximation to the steady-state gradients of both temperature and concentration imposed in the horizontal direction in the rectangular cavity. Lee er al. [13] and Lee and Hyun[14] observed the layered flow structure in the rectangular enclosures of aspect ratio 2.0 and 0.2.Mamou et al. [15] have reported an analytical and numerical study of double-diffusive convection in a vertical enclosure. Mamou and Vasseur [16] have discussed hysteresis effect on thermosolutal convection with opposed buoyancy forces in inclined enclosures.

Natural convection in an enclosure with partially active walls is studied by Nithyadevi et al. and Kandaswamy et al. [17] without buoyancy ratio and mass transfer. The present study describes the double-diffusive natural convection in a rectangular cavity with partially active side walls for nine different heating locations. That is, for the hot region located at the top, middle and bottom and the cold region moved from bottom to top, to locate the regions where the heat and mass transfer rate is maximum and minimum. The results are displayed graphically in terms of the streamlines, isotherms and isoconcentration, which show the effect of the aspect ratio with different heating locations of the side walls.

2. Mathematical formulation

A schematic diagram of the two-dimensional rectangular cavity of length L and height H filled with moist air, with a concentration, it can be taken $Pr = 0.71$and $Sc = 2$ is shown in Fig. 1.The partiallythermally active side walls of the cavity are maintained at two different but uniform temperatures and concentration, namely, T_h and $T_C(T_h > T_C)$, c_h and $c_l(c_h > c_l)$, respectively.The inactive parts of the side walls and horizontal walls y = 0 and y = H are thermally insulated. Nine different cases will be studied here. That is, for the hot region located at the top, middle and bottom and the cold region moved from bottom to top. The length of the thermally active part is $h = \frac{H}{2}$.The gravity acts normal to the x-axis. The fluid is assumed to be incompressible, Newtonian, and viscous. The viscous dissipation is assumed to be negligible. The heat flux driven by concentration gradients (thermal diffusion or Soret effect) and the mass flux driven by temperature gradients (diffusion thermo or Dufour effect) are neglected.

The Boussinesq approximation with opposite thermal and solute buoyancy forces is used for the body force terms in the momentum equations.

The governing equations for the problem under consideration are based on the balance laws of mass, momentum, energy, and concentration in two dimensions. Representing the position through Cartesian coordinate system and Taking into account the assumptions mentioned above, these equations can be written in dimensional form as

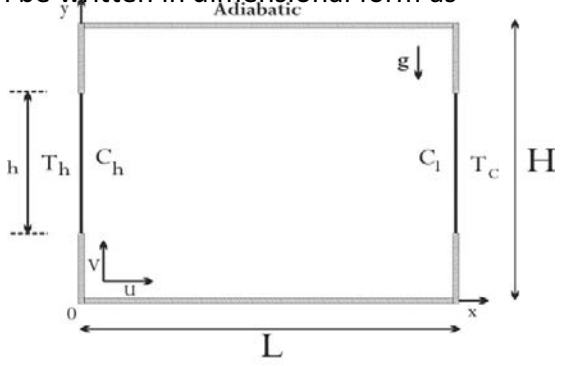

Fig. 1. Physical configuration.

Nomenclature

c	concentration
C	dimensional concentration
D	mass diffusivity
g	acceleration due to gravity
Gr_T	thermal Grashof number
Gr_c	solutal Grashof number
H	height of the cavity
L	length of the cavity
N	buoyancy ratio
Nu	local Nusselt number
$\overline{Nu}$	average Nusselt number
p	pressure
Pr	Prandtl number
Sc	Schmidt number
Sh	local Sherwood number
$\overline{Sh}$	average Sherwood number
t	time
T	temperature
u, v	velocity components
U, V	dimensionless velocity components
x, y	coordinates
X, Y	dimensionless coordinates

Greek symbols

α	thermal diffusivity
β_T	coefficient of thermal expansion
β_c	coefficient of solutal expansion
ν	kinematic viscosity
θ	dimensionless temperature
ω	vorticity
ψ	stream function
Ψ	dimensionless stream function
ρ	density
τ	dimensionless time
ξ	dimensionless vorticity

Subscripts

c	cold wall

h	hot wall and high concentration
l	low concentration

$$\frac{\partial u}{\partial x} + \frac{\partial v}{\partial y} = 0 \qquad (1)$$

$$\frac{\partial u}{\partial t}+u\frac{\partial u}{\partial x}+v\frac{\partial u}{\partial y}=-\frac{1}{\rho_0}\frac{\partial \mathrm{P}}{\partial x}+\nu\left[\frac{\partial^2 u}{\partial x^2}+\frac{\partial^2 u}{\partial y^2}\right] \quad (2)$$

$$\frac{\partial v}{\partial t}+u\frac{\partial v}{\partial x}+v\frac{\partial v}{\partial y}=-\frac{1}{\rho_0}\frac{\partial \mathrm{P}}{\partial y}+\nu\left[\frac{\partial^2 v}{\partial x^2}+\frac{\partial^2 v}{\partial y^2}\right]-\frac{\rho}{\rho_0}g \quad (3)$$

$$\frac{\partial \mathrm{T}}{\partial t}+u\frac{\partial \mathrm{T}}{\partial x}+v\frac{\partial \mathrm{T}}{\partial y}=\alpha\left[\frac{\partial^2 \mathrm{T}}{\partial x^2}+\frac{\partial^2 \mathrm{T}}{\partial y^2}\right] \quad (4)$$

$$\frac{\partial c}{\partial \mathrm{t}}+u\frac{\partial \mathrm{c}}{\partial x}+\mathrm{v}\frac{\partial \mathrm{c}}{\partial y}=\mathrm{D}\left[\frac{\partial^2 \mathrm{c}}{\partial x^2}+\frac{\partial^2 \mathrm{c}}{\partial y^2}\right] \quad (5)$$

The mixture density is assumed to be uniform over all the cavity, exception made to the buoyancy term, in which it is taken as a function of both the temperature and concentration levels through the Boussinesq approach.

where

$$\rho=\rho_0[1-\beta_{\mathrm{T}}(\mathrm{T}-\mathrm{T}_c)+\beta_{\mathrm{C}}(\mathrm{c}-\mathrm{c}_l)] \quad (6)$$

The appropriate initial and boundary conditions are

$$t=0: u=v=0, T=T_c, C=C_l, \qquad 0\le x\le L, 0\le y\le H,$$

$$t>0: u=v=0, T=T_h, C=C_h, \qquad \text{on the hot wall, } x=0,$$

$$T=T_c, C=C_l, \qquad \text{on the cold wall, } x=L,$$

$$\frac{\partial T}{\partial x}=0, \frac{\partial C}{\partial x}=0, \qquad x=0 \text{ and } L,$$

$$\frac{\partial T}{\partial y}=0, \frac{\partial C}{\partial y}=0, \qquad y=0 \text{ and } H.$$

Introducing the following non-dimensional variables

$$\tau=\frac{t}{L^2/\nu}, \quad X=\frac{x}{\mathrm{L}}, \quad Y=\frac{y}{H}, \quad U=\frac{u}{\nu/L}, \quad V=\frac{v}{\nu/L}\frac{L}{H},$$

$$\Psi=\frac{\psi}{\nu}\frac{L}{H}, \quad \xi=\frac{\omega}{\nu/HL}, \quad \theta=\frac{\mathrm{T}-\mathrm{T}_c}{\mathrm{T}_h-\mathrm{T}_c}, \quad C=\frac{\mathrm{c}-\mathrm{c}_l}{\mathrm{c}_h-\mathrm{c}_l}.$$

we get the vorticity–stream function formulation of the above problems (1)–(5) as

$$\frac{\partial \xi}{\partial \tau} + U\frac{\partial \xi}{\partial X} + V\frac{\partial \xi}{\partial Y} = \frac{\partial^2 \xi}{\partial X^2} + \frac{1}{Ar^2}\frac{\partial^2 \xi}{\partial Y^2} + ArGr_T\frac{\partial \theta}{\partial X} - ArGr_C\frac{\partial C}{\partial X} \quad (7)$$

$$\frac{\partial \theta}{\partial \tau} + U\frac{\partial \theta}{\partial X} + V\frac{\partial \theta}{\partial Y} = \frac{1}{\mathrm{Pr}}\left[\frac{\partial^2 \theta}{\partial X^2} + \frac{1}{Ar^2}\frac{\partial^2 \theta}{\partial Y^2}\right] \quad (8)$$

$$\frac{\partial C}{\partial \tau} + U\frac{\partial C}{\partial X} + V\frac{\partial C}{\partial Y} = \frac{1}{Sc}\left[\frac{\partial^2 C}{\partial X^2} + \frac{1}{Ar^2}\frac{\partial^2 C}{\partial Y^2}\right] \quad (9)$$

Where

$$-\xi = Ar^2\frac{\partial^2 \Psi}{\partial X^2} + \frac{\partial^2 \Psi}{\partial Y^2} \quad (10)$$

The initial and boundary conditions in the dimensionless form are

$\tau = 0$: $\Psi = 0, \theta = 0, C = 0,$ $0 \le X \le 1, 0 \le Y \le 1,$

$\tau > 0$: $\Psi = \frac{\partial \Psi}{\partial Y} = 0, \theta = 1, C = 1,$ on the hot part $X = 0,$

$\Psi = \frac{\partial \Psi}{\partial Y} = 0, \theta = 0, C = 0,$ on the cold part $X = 1,$

$\Psi = 0, \frac{\partial \theta}{\partial X} = 0, \frac{\partial C}{\partial X} = 0,$ at $X = 0$ and 1,

$\Psi = \frac{\partial \Psi}{\partial Y} = 0, \frac{\partial \theta}{\partial Y} = 0, \frac{\partial C}{\partial Y} = 0,$ at $Y = 0$ and 1.

The non-dimensional parameters that appear in the equations are $Gr_T = \frac{g\beta_T \Delta T L^3}{\nu^2}$ the thermal Grashof number, $Gr_c = \frac{g\beta_c \Delta C L^3}{\nu^2}$ the solutal Grashof number, $N = \frac{\beta_c(c_h - c_l)}{\beta_T(T_h - T_c)}$ the buoyancy ratio, $Pr = \frac{\nu}{\alpha} = 0.71$ the Prandtl number, $Sc = \frac{\nu}{D} = 2$ the Schmidt number, g the acceleration due to gravity, ν the kinematic viscosity, α the thermal diffusivity, D the mass diffusivity, β_T coefficient of volumetric expansion with temperature, β_c coefficient of volumetric expansion with concentration, T temperature , θ dimensionless temperature, t time, and $Ar = \frac{H}{L}$ the aspect ratio.

The local Nusselt number and Sherwood number is defined by $Nu = -\frac{\partial \theta}{\partial X}|_{X=0}, Sh = -\frac{\partial C}{\partial X}|_{X=0}$, resulting in the average Nusselt number and Sherwood number as $\overline{Nu} = \frac{1}{Ar}\int_0^{Ar} Nu\ dY, \overline{Sh} = \frac{1}{Ar}\int_0^{Ar} Sh\ dY.$

3. Method of solution

The governing equations along with the boundary conditions are solved numerically, employing finite-difference techniques. The region of interest was covered with 'm' vertical and 'n' horizontal uniformly spaced grid lines. The vorticity transport, energy and mass equations are solved using the ADI (Alternating Direction Implicit) method and the stream function equation is solved by SOR (successive over-relaxation) method. The over-relaxation parameter is chosen to be 1.8 for stream function solutions. The buoyancy and diffusive terms are discretized by using central differencing while the use of upwind differencing is preferred for convective terms for numerical stability. Starting from arbitrarily specified initial values of variables, the discretized transient equations are then solved by marching in time until an asymptotic steady-state solution is reached. Convergence of iteration for stream function solution is obtained at each time step. The following criterion is employed to check for steady-state solution

$$\frac{\sum\sum\left|\Phi_{i,j}^{k+1}-\Phi_{i,j}^{k}\right|}{|\Phi|_{max}\times m\times n}\leq\varepsilon \qquad (11)$$

where Φ stands for Ψ, ξ or θ; k refers to time and i and j refer to space coordinates. The value of ε is chosen as 10^{-5}. The time step used in the computations is varied between 0.00001 and 0.004 depending on Grashof number and mesh size.

The numerical solutions are found for different grid systems from 21× 21 to 101 × 101 for Ar=1 and it is observed that a further refinement of grids from 41×41 to 101 × 101 does not have a significant effect on the results in terms of average Nusselt and Sherwood number and the maximum value of the stream function. Based on this observation, a uniform grid of 41×41 points is used for all of the calculations for Ar = 1. Similar grid dependency studiers carried out for the other aspect ratios and an optimum grid size is obtained for a each aspect ratio.

4. Results and discussion

Numerical study is conducted for different heating locations, thermal Grashof numbers, Buoyancy ratio number and aspect ratios. The results are presented in the form of streamlines, isotherms, isoconcentration and mid-height velocity profiles to show the fluid flow, heat and mass transfer phenomena in steady states. The rate of heat and mass transfer in the enclosure is measured in terms of the average Nusselt number and average Sherwood number.

The flow pattern, isotherms and isoconcentration for different heating locations, Ar = 2 and Gr = 10^6 and N = 0.2 are displayed in Figs. 2,3 and 4a–i.The flow is unicellular with clockwise rotation. The mirror image of the top–top active locations exists for bottom– bottom thermally active locations, as seen in Fig. 2a and 2i.When the heating location is either top–middle or middle– bottom, the flow is activated around the active zones while the remaining portion of the cavity remains stagnant. It is observed in Fig. 2c that a peculiar phenomenon occurs for the top–bottom thermally active location. The flow is in two cells and centers of the cells are located near the thermally active parts of the side walls. When compared to other positions the heat transfer rate is much less in this case. There exist some small eddies within the clockwise

rotating eddy, occupying the whole cavity for all the remaining thermally active zones. The heat transfer rate is maximum at the bottom–top active location.

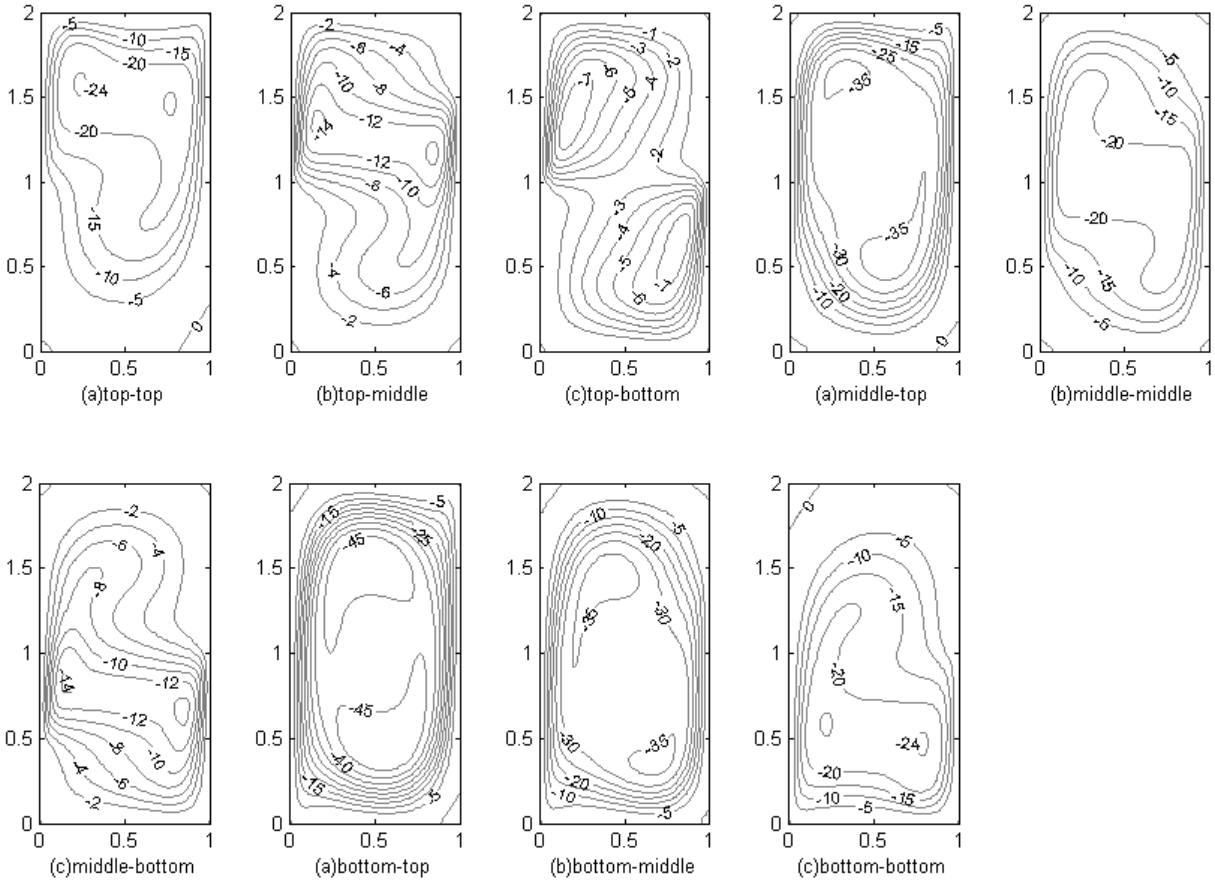

Fig. 2. Streamlines for all heating location, Ar = 2, N = 0.2 and Gr = 10^6.

Fig. 3a depicts the convection mode of isotherms mostly at the top region where the active walls are located. When the cold active wall moves from top to bottom, Fig. 3b shows the modifications that the isotherms are transformed towards conduction at the central region and convection near the active locations. As the cold wall is moved to the bottom, the isotherms predict almost conduction at the middle of the cavity. In this case, the circulation rate and velocity are very low compared to all the other cases. Fig. 3i and f seems to be the mirror images of Fig. 3a and b, respectively. In the middle–top and bottom–middle active locations there is a boundary layer formed at the active walls and the existence of convection is seen from the isotherms of Fig. 3d and h. In Fig. 3e, the middle–middle active location exhibits convection near the active locations. Strong thermal boundary layers are formed at the active locations as seen in Fig. 3g.The circulation rate and the heat transfer rate are maximum in this case compared to all the other cases.

Fig. 4a–i depicts the convection mode of isoconcentration. As you see the isoconcentration has the same behaviour as isothermal and this is, because of the similarity of energy equation and

mass transfer equation. According to Schmidt number which is greater than Prandtl number, the thermal diffusivity has greater effect than the mass diffusivity on fluid. So, formed solutal boundary layer in Fig. 4d and h, in relation with formed thermal boundary layer in Fig. 3d and h is thinner. Fig. 4i and f seems to be the mirror images of Fig. 4a and b, respectively. In Fig. 4e, the middle–middle active location exhibits convection near the active locations. Strong solutal boundary layers are formed at the active locations as seen in Fig. 4g. The circulation rate and the mass transfer rate are maximum in this case compared to all the other cases.

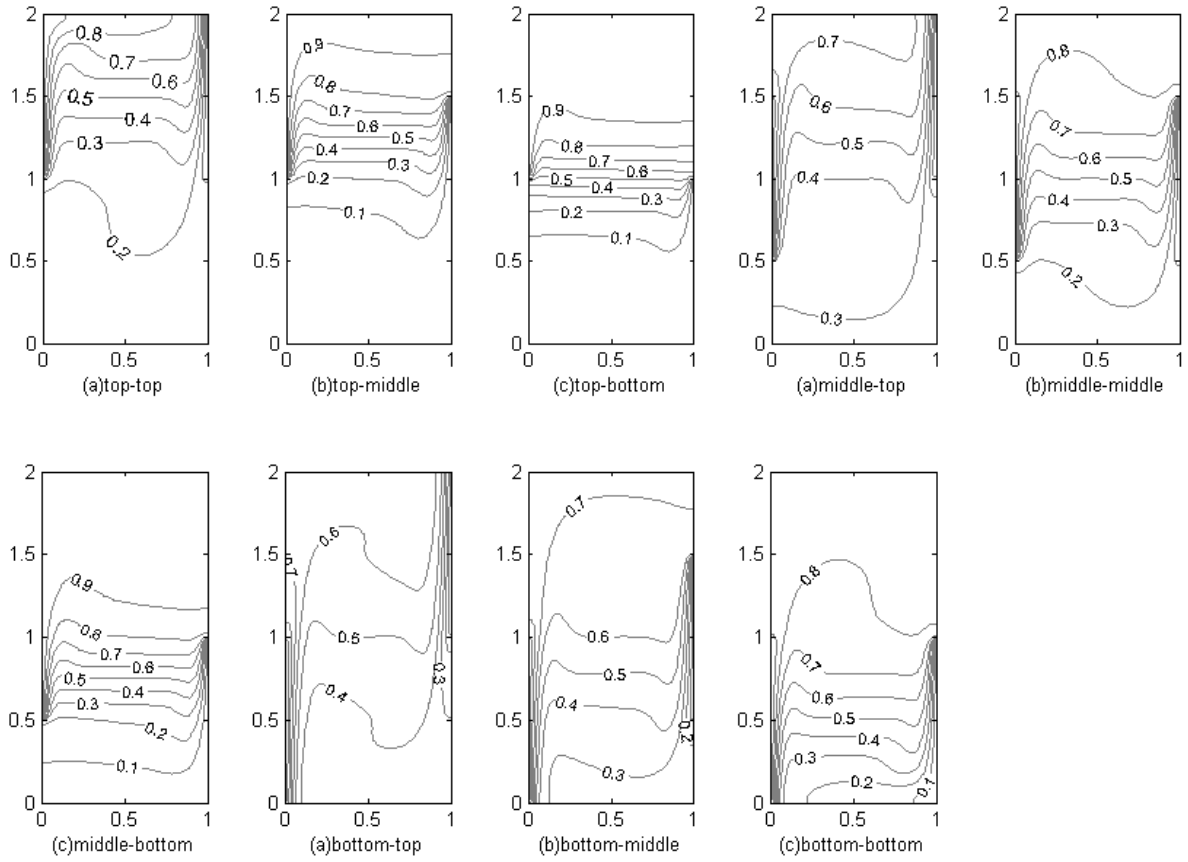

Fig. 3. Isotherms for all heating location, Ar = 2, N = 0.2 and Gr = 10^6.

The flow patterns for the middle–middle thermally active location, different aspect ratios and $Gr = 5 \times 10^5$are displayed in Fig. 5a–e. When Ar = 0.5, in Fig. 5a, a single cell pattern is observed. For the case of square cavity, there exist two inner cells each at the top left and bottom right corners of the cavity. The remaining two corners are less activated but this type of behaviour does not exist in the case of rectangular cavities. The two inner cells are moved to the active locations parts of the cavity when Ar = 2. This is due to the ominating buoyancy force inside the cavity. Further increasing the aspect ratio to 5 the recirculating zones in the middle of the cavity disappear.

The isotherms for the middle–middle thermally active location, different aspect ratios and $Gr = 5 \times 10^5$ are presented in Fig. 6a–e. For all the aspect ratios, a thermal boundary layer

exists along the active zones. Large velocity and temperature gradients characterize the region immediately adjacent to the thermally active side wall locations while negligible gradients (normal to the hot/cold wall location) prevail in the rest of the cavity. Such behaviour is indicative of the thermal boundary layer structure.

The isoconcentration for the middle–middle thermally active location, different aspect ratios and $Gr = 5 \times 10^5$are presented in Fig. 7a–e. As you see the isoconcentration has the same behaviour as isothermal but the change are more.

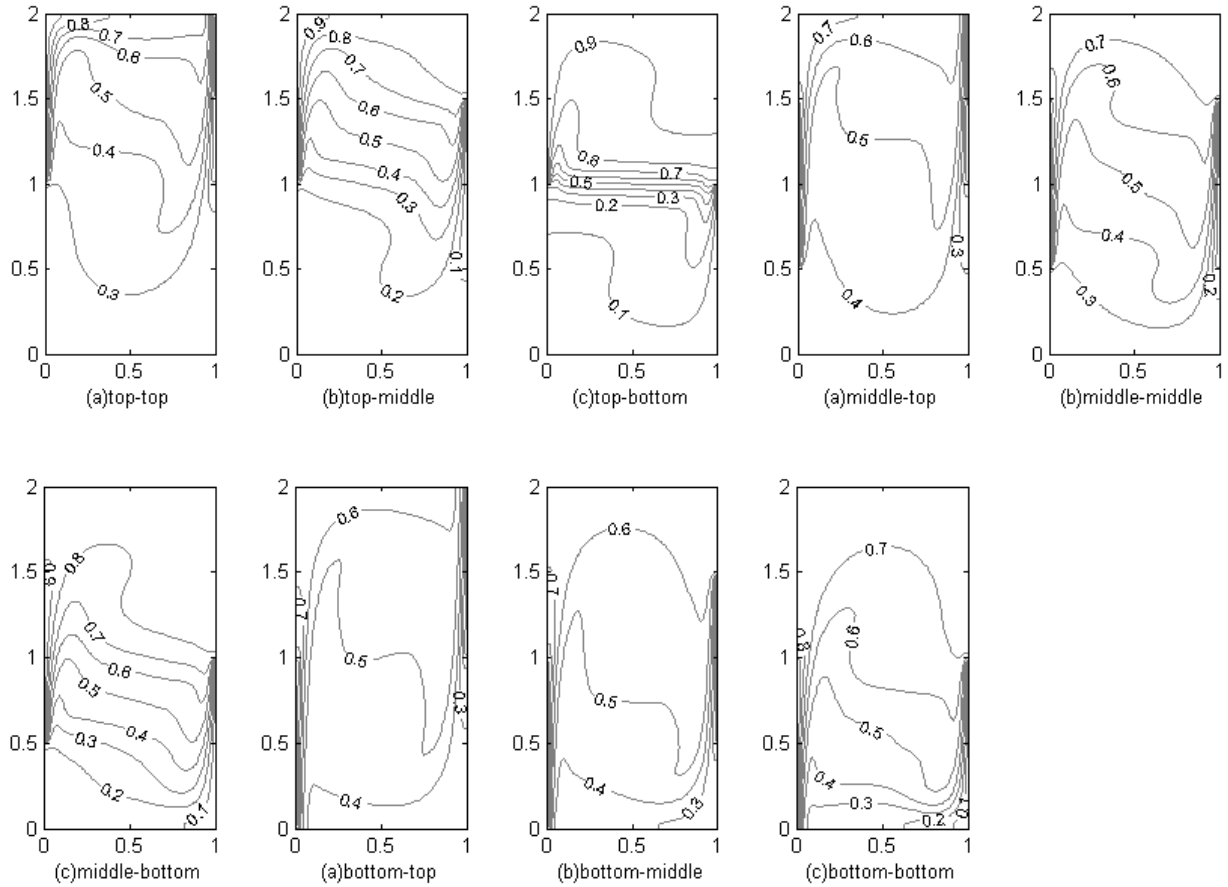

Fig. 4.Isoconcentration for all heating location, Ar = 2, N = 0.2 and Gr = 10^6.

Figs. 8, 9 and 10a–d show the streamlines, isotherms and isoconcentration for different Grashof numbers, bottom–top thermally active locations and Ar = 3. There exists a clockwise rotating cell in the middle portion of the cavity for Gr = 10^3. When Gr = 10^4 and Gr = 10^5 the circulation rate of the eddy is increased. Further increasing Gr = 10^6, there exist two secondary cells inside a large primary celland occupies the whole cavity.

The time history of the average Nusselt and Sherwood number for different aspect ratios and top-top active locations are displayed in Fig. 11. Thus the average Nusselt and Sherwood

number is increased as the aspect ratio increases. Increasing the aspect ratio increases the time to reach the steady state situation of the solution.

Fig. 12 shows the mid-height velocity, temperature and concentration profile for different aspect ratios and middle–middle thermally active locations. The increase in the vertical velocity of the fluid particles at mid-height of the cavity for increasing aspect ratio near the active locations is shown in Fig. 12–a.

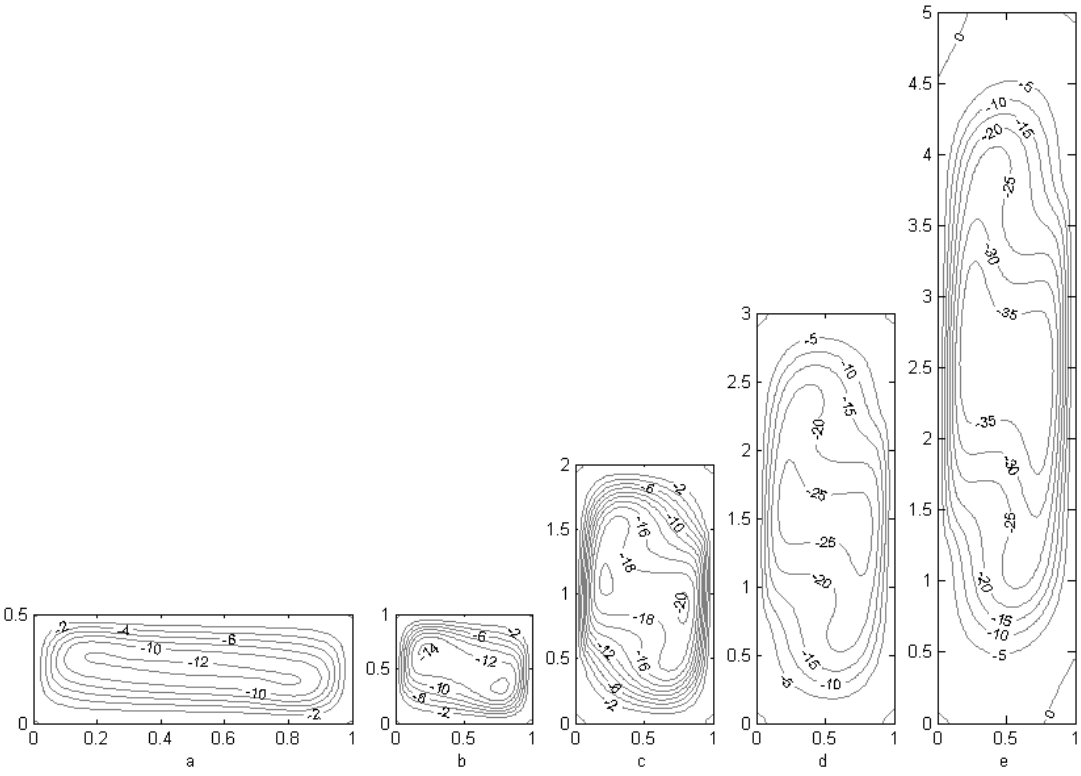

Fig. 5. Streamlines for middle-middle heating location, aspect ratios 0.5, 1, 2, 3 and 5 and N = 0.2 and Gr = 5×10^5.

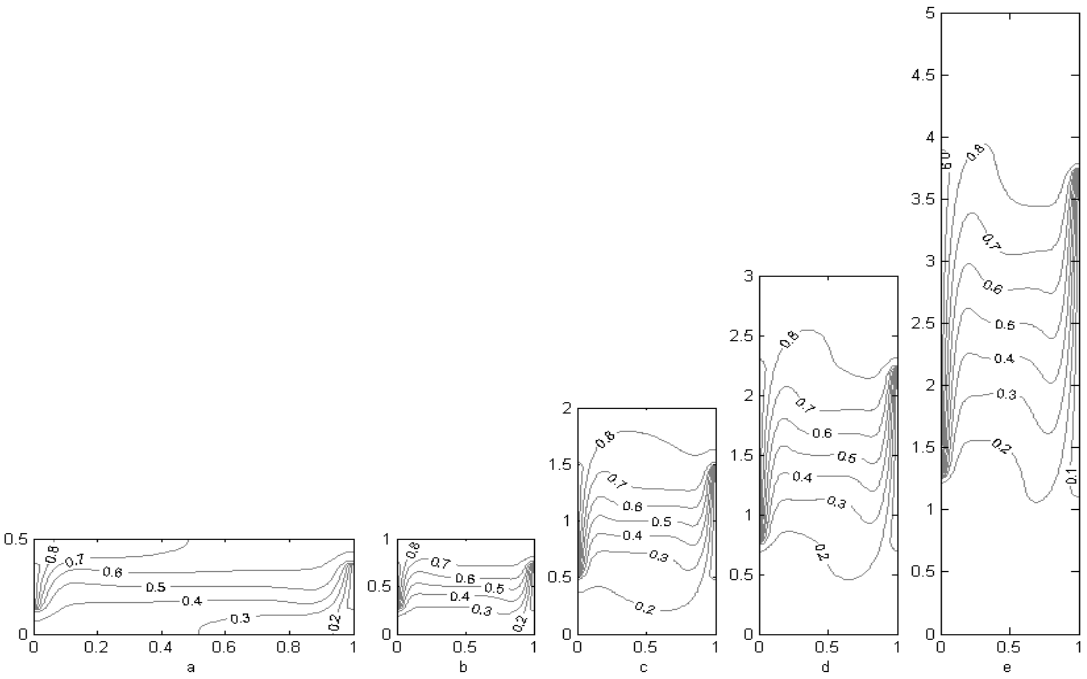

Fig. 6. Isotherms for middle-middle heating location, aspect ratios 0.5, 1, 2, 3 and 5 and N = 0.2 and Gr = 5×10^5.

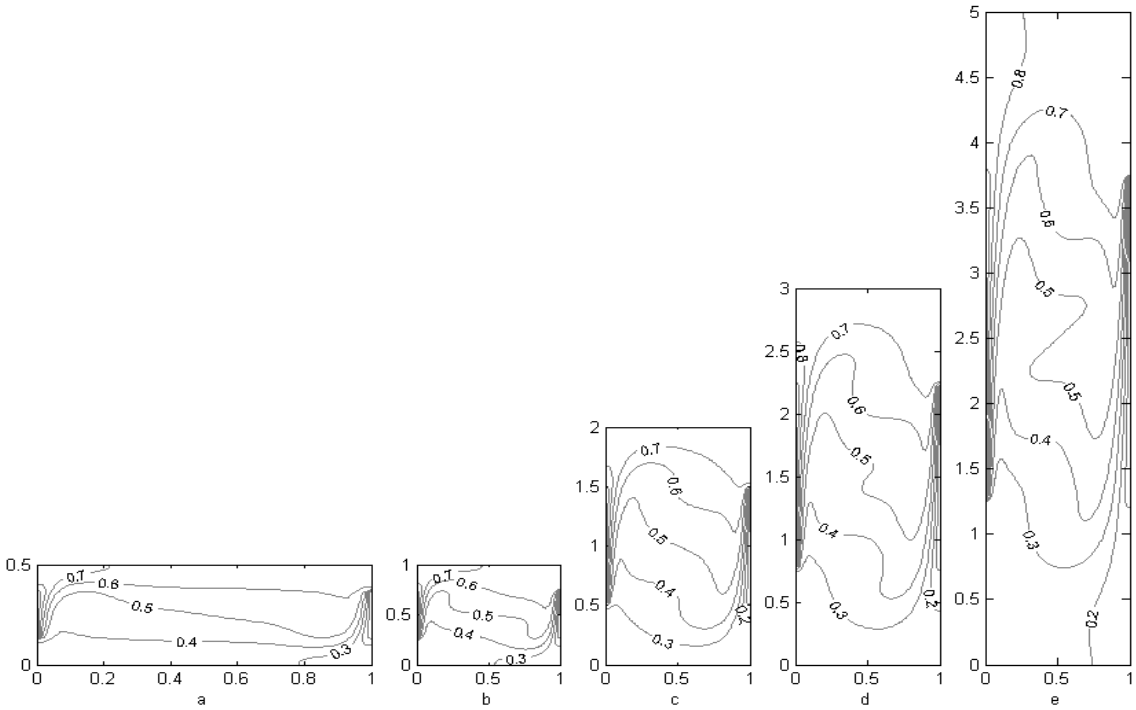

Fig. 7.Isoconcentration for middle-middle heating location, aspect ratios 0.5, 1, 2, 3 and 5 and N = 0.2 and Gr = 5×10^5.

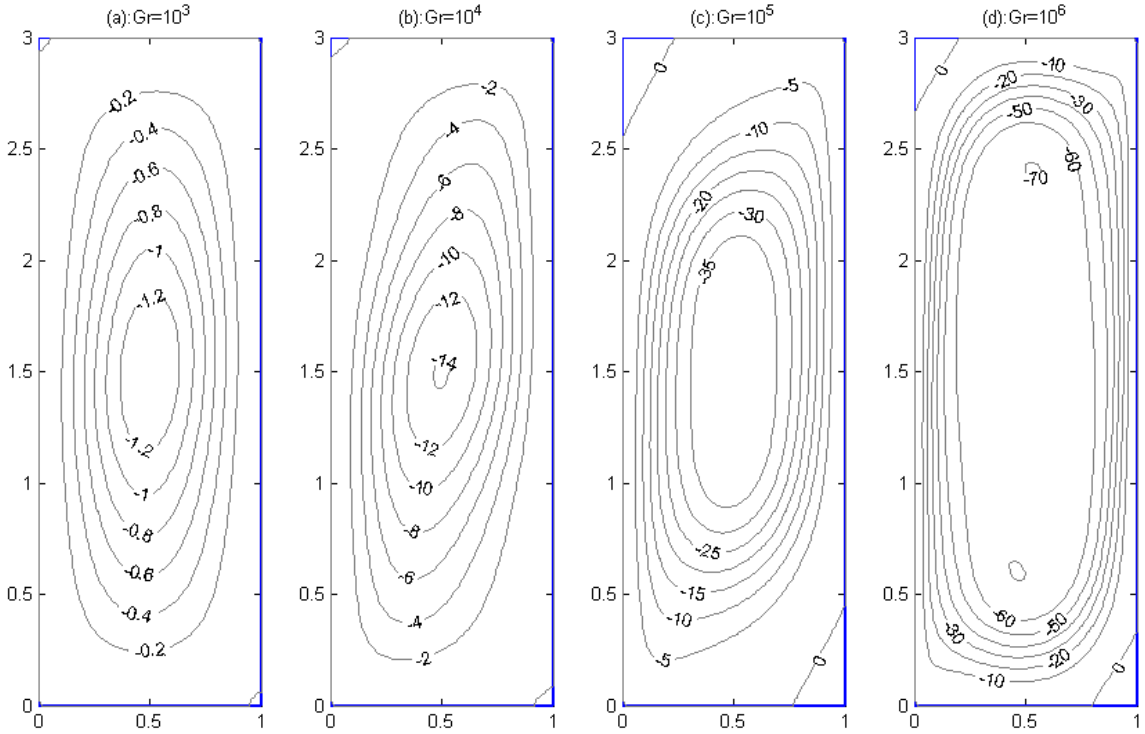

Fig.8Streamlines for bottom-top heating location for different Grashof numbers and Ar = 3.

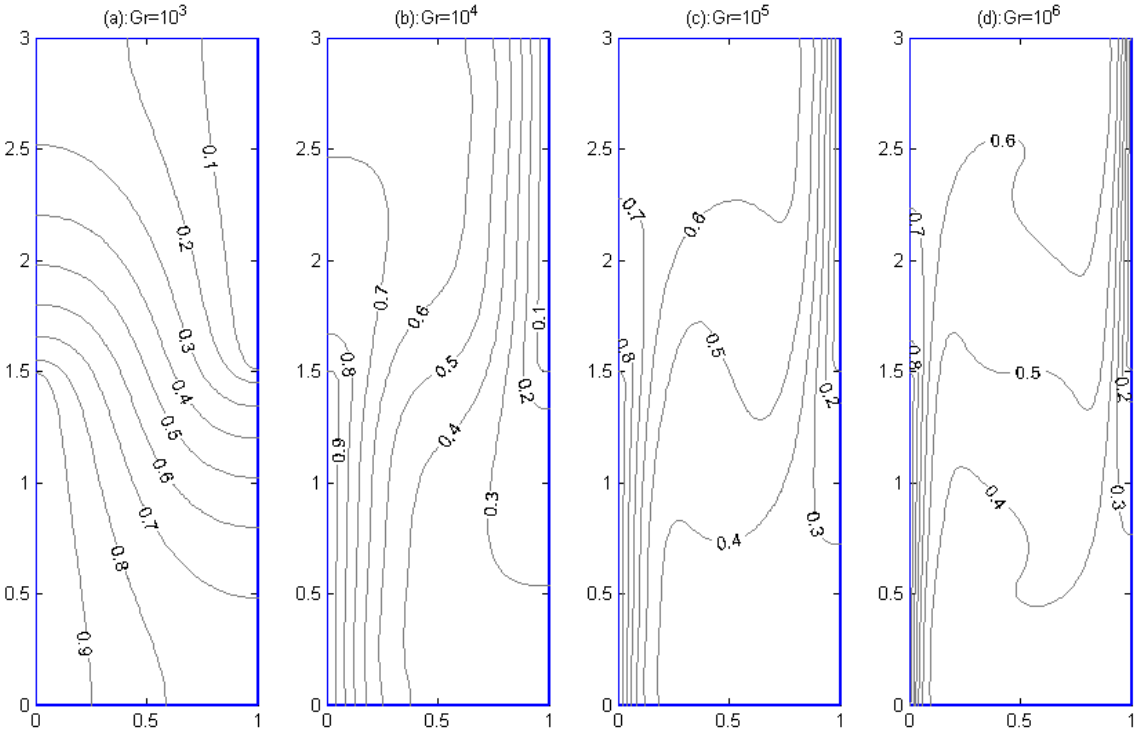

Fig. 9. Isotherms for bottom-top heating location for different Grashof numbers and Ar = 3.

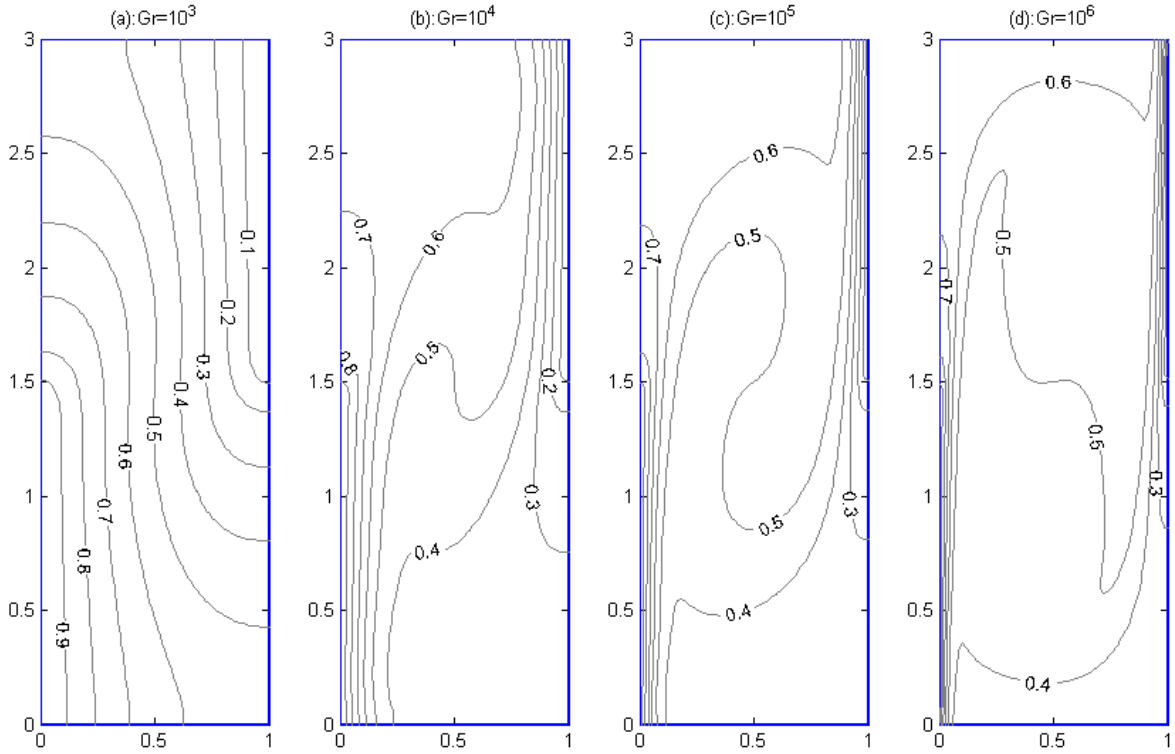

Fig. 10. Isoconcentration for bottom-top heating location for different Grashof numbers and Ar = 3.

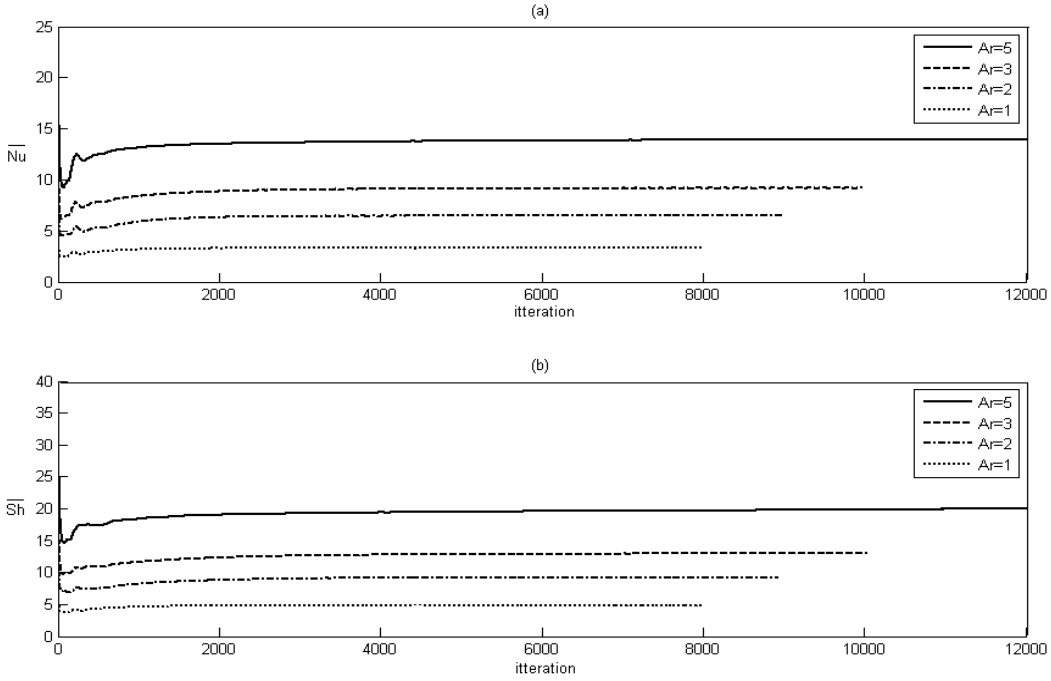

Fig. 11. Time history of average Nusselt and Sherwood number for different, aspect ratios and Gr = 10^6.

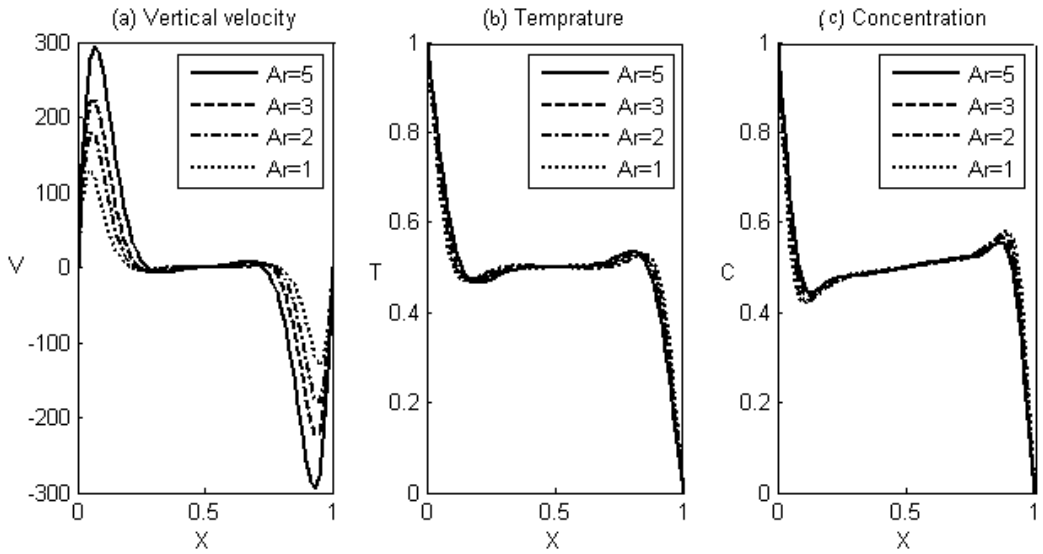

Fig. 12. Mid-height velocity, temperature and concentration profile for middle-middle heating location.

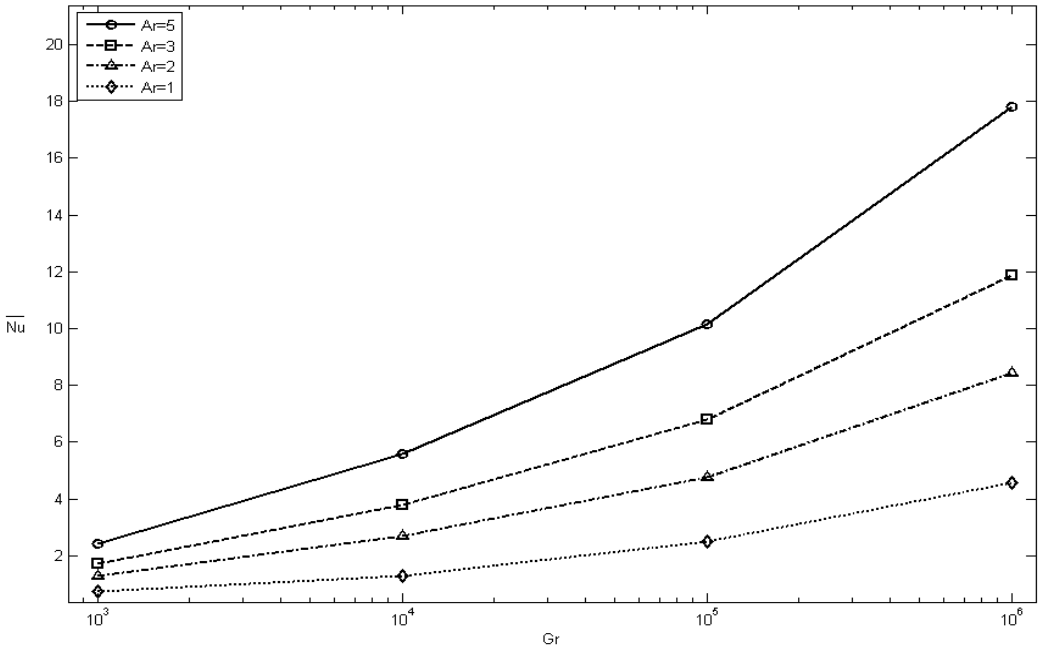

Fig. 13. Average Nusselt number for different aspect ratios.

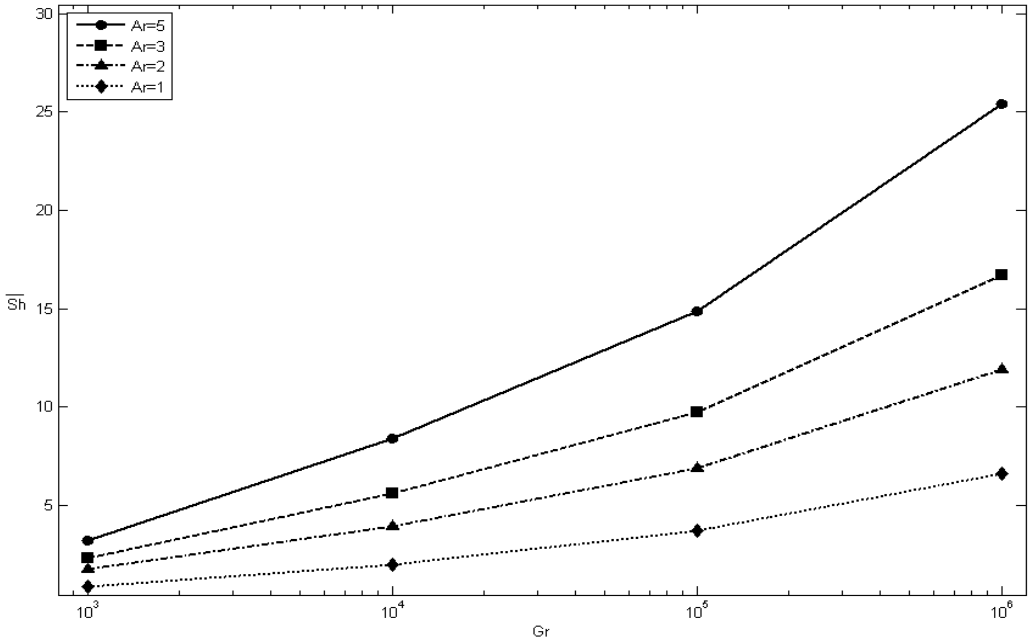

Fig. 14. Average Sherwood number for different aspect ratios.

Its clear that in Fig. 12–b and c the increasing aspect ratio in middle-middle thermally active locations has a little effect on thickness thermal boundary layer and thickness solutal boundary layer but for different heating locations specially bottom-top thermally active locations, the increasing aspect ratio causes the increasing of thickness thermal boundary layer and solutal boundary layer. Its obvious that in Fig. 12–b, the thickness thermal boundary layer is more than thickness solutal boundary layer in Fig. 12–c but the change are less.

Average Nusselt and Sherwood number for different aspect ratios, different Grashof numbers and middle–top thermally active locations is depicted in Fig. 13 and 14. The heat and mass transfer rate is increased by increasing both the aspect ratio and the Grashof number.

In order to evaluate how the aspect ratio and different heating locations affect the heat and mass transfer rate, the average Nusselt and Sherwood number is plotted as a function of aspect ratio for different thermally active zones in Figs. 15 and 16a–c. Heat and mass transfer rate is increased on increasing the aspect ratio. There is no considerable variation in the average Nusselt and Sherwood number for $\mathrm{Ar} \leq 1$ when the heating locations are changed. But the variation in the average Nusselt and Sherwood number when changing the heating location is increased by increasing the aspect ratio, Figs. 15a–c and 16a–c. The heat and mass transfer rate is enhanced when a cooling location is at the top of the enclosure. When changing the cooling location from bottom to top the average Nusselt and Sherwood number is increased by increasing the aspect ratio. It is clearly seen from Figs. 15a–c and 16a–c.

As it is shown in Fig. 17, the results obtained in this paper are in good agreement with the reference [17]. For example, the increase in the vertical velocity of the fluid particles at mid-

height of the cavity aspect ratio with (that is shown in in this article, is in

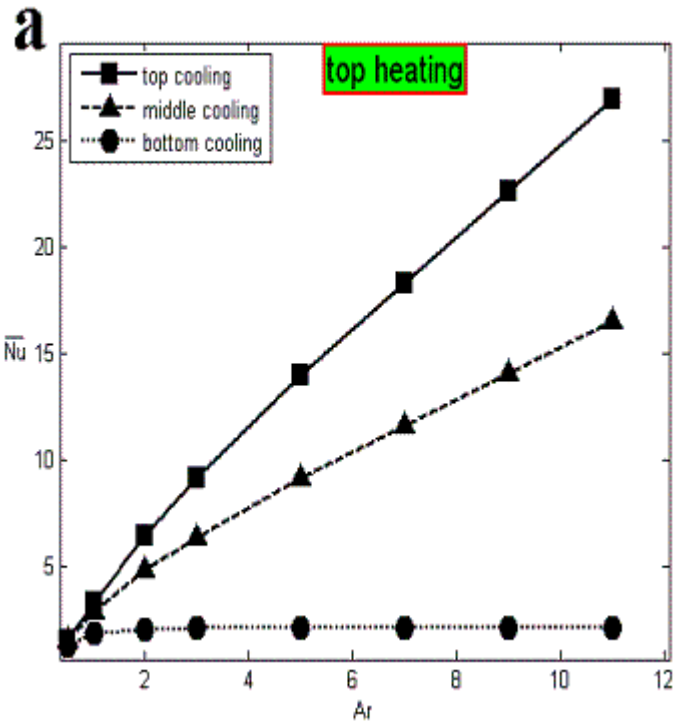

for increasing buoyancy ratio Fig. 12a) obtained common with [17].

5. Conclusions

The heat and mass for the bottom–top location while the transfer rate is poor thermally active to reach the steady the solution is with increase in the vertical velocity of mid-height of the increase with aspect ratio. The transfer rate is transfer rate is high thermally active heat and mass in the top–bottom location. The time state situation of found to increase aspect ratio. The the fluid particles at cavity is found to increase in the heat and mass found to increase with increase in the aspect ratio. There is no considerable variation in the heat and mass transfer rate for $\mathrm{Ar} \leq 1$ when the heating locations are changed.

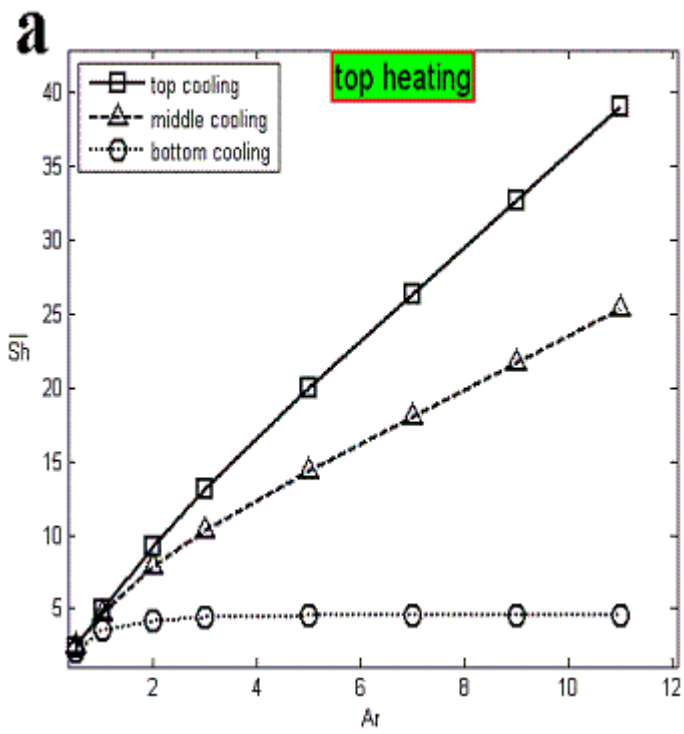

Fig. 15. Average Nusselt number for different heating location.

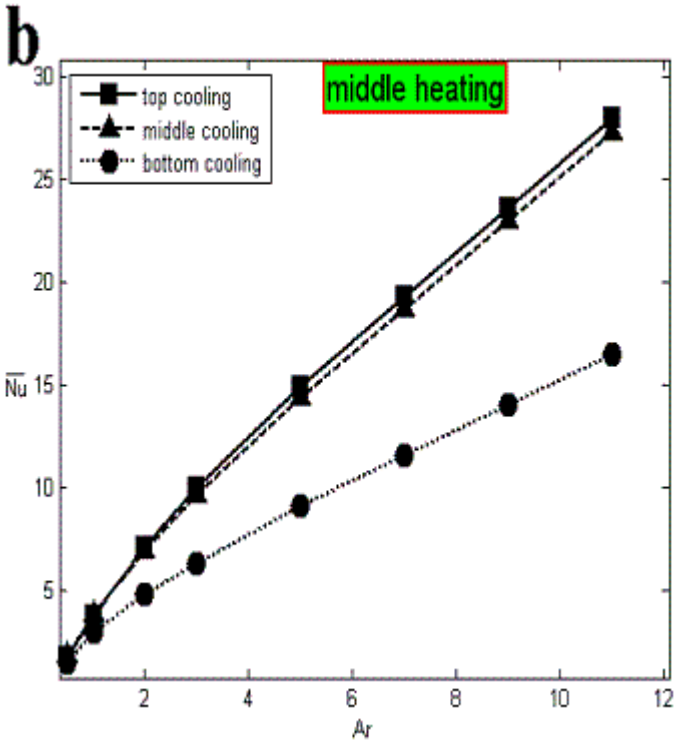

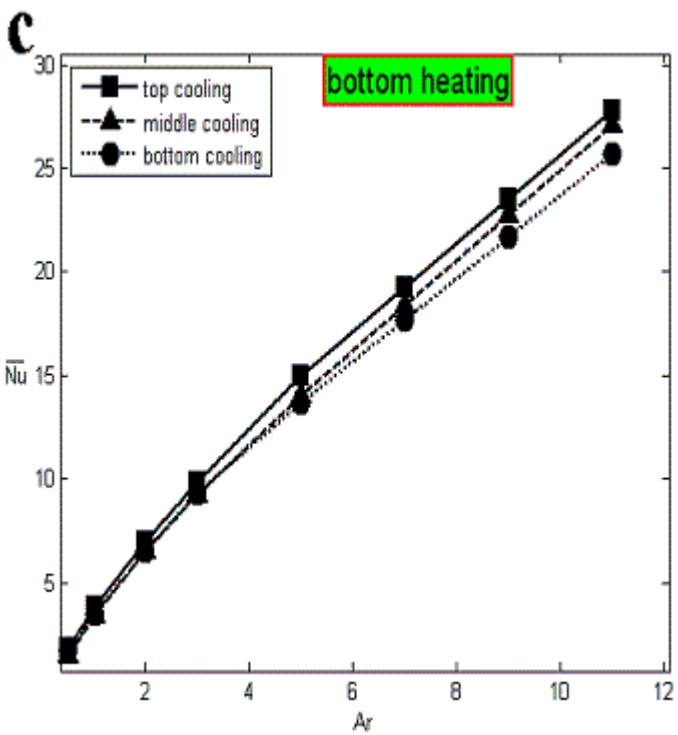

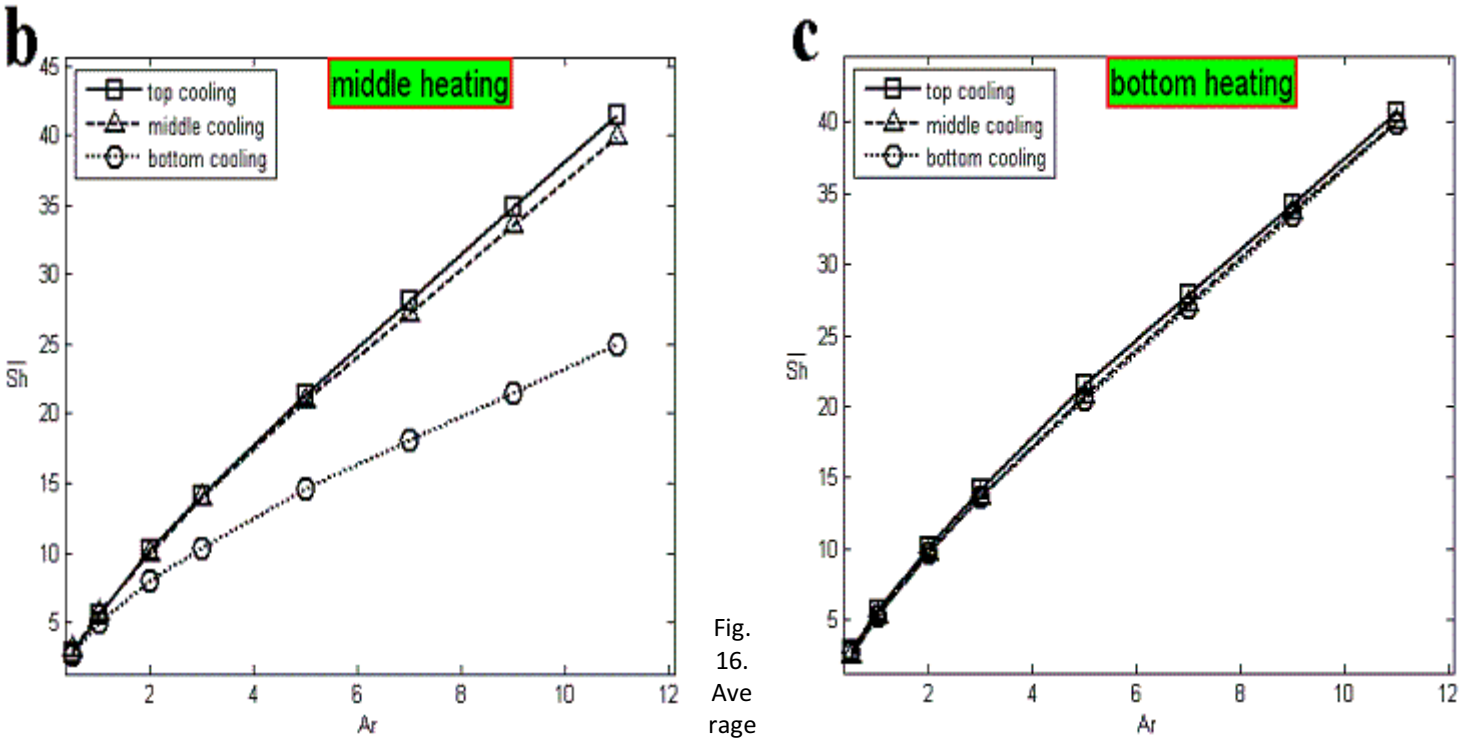

Fig. 16. Average Sherwood number for different heating location.

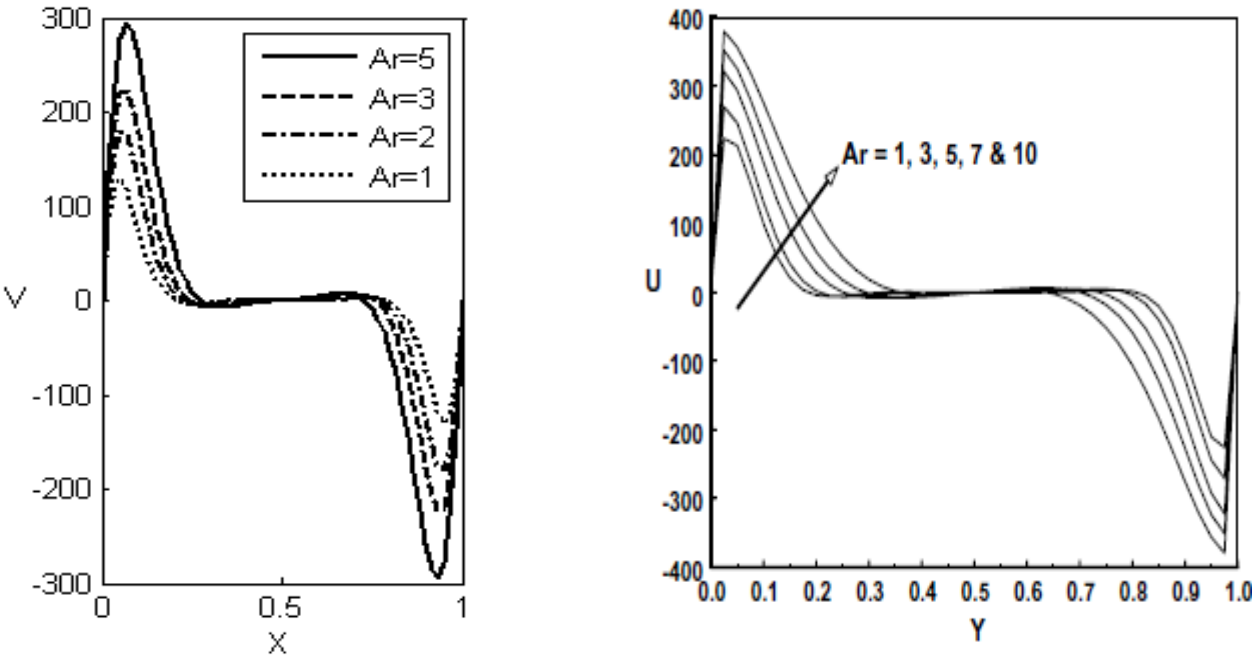

(a) This paper (b) Ref. [17]

Fig 17. The comparison between the results obtained in this paper and Ref. [17].

References

[1] J. S. Turner, Buoyancy Effects in Fluids. Cambridge University Press, London (1979).

[2] S. Ostrach. Fluid mechanics in crystal growth-The 1982 Freeman Scholar Lecture, J. Fluids Engng 105, 5-20 (1983).

[3] B. Gebhart and L. Pera, The nature of vertical natural convection flows resulting from the combined buoyancy effects of thermal and mass diffusion, Int. J. Heat Mass Transfer 14,2025-2050 (1971).

[4] A. Bejan. Mass and heat transfer by natural convection in a vertical cavity, In. J. Heat Fluid Flow 6, 149-159 (1985).

[5] 0. V. Trevisan and A. Bejan, Combined heat and mass transfer by natural convection in a vertical enclosure ASME J. Heat Transfer 109, 104-112 (1987).

[6] T. F. Lin, C. C. Huang and T. S. Chang, Transient binary mixture natural convection in square enclosures, Int. J. Heat Muss Transfer 33, 287-299 (1990).

[7] P. Ranganathan and R. Viskanta, Natural convection of a binary gas in rectangular cavities, ASME-JSME Thermal Engng Joint Conf., Hawaii (1987).

[8] C. Beckermann and R. Viskanta, Double-diffusive convection during dendritic solidification of a binary mixture, PhysicoChem. Hydrodyn.10, 195-213 (1988).

[9] C. Y. Hu and M. M. El-Wakil, Simultaneous heat and mass transfer in a rectangular cavity, Proc. 5th Int. Heat Transfer Conf., Vol. 5, pp. 24-28 (1974).

[10] C. Benard, D. Gobin and J. Thevenin, Thermosolutal natural convection in a rectangular enclosure : numerical results, In Heat Transfer in Convective Flows (Edited by R. K. Shah), ASME HTD-Vol. 107, pp. 249-254 (1989).
[11] L. W. Wang, Y. Kamotani and S. Ostrach, Experimental study of natural convection in a shallow horizontal cavity with different end temperatures and concentrations, Report FTAS/TR-82-164, Case Western Reserve University (1983).
[12] Y. Kamotani, L. W. Wang, S. Ostrach and D. Jiang, Experimental study of natural convection in shallow enclosures with horizontal temperature and concentration gradients, Int. J. Heat Mass Transfer 28, 165-173 (1985).
[13] J. Lee, M. T. Hyun and K. W. Kim, Natural convection confined fluids with combined horizontal temperature in and concentration gradients, Int. J. Heat Mass Transfer31, 1969-1977 (1988).
[14] J. Lee and M. T. Hyun, Experiments on thermosolutal convection in a shallow rectangular enclosure, ExP. Thermal Fluid Sci. 1,259-265 (1988).
[15] Mamou M., Vasseur P., Bilgen E., Analytical and numerical study of double diffusive convection in a vertical enclosure, Heat Mass Tran. 32 (1996) 115–125.
[16] Mamou M., Vasseur P., Hysteresis effect on thermosolutal convection with opposed buoyancy forces in inclined enclosures, Int. Comm. Heat Mass Tran. 26 (1999) 421–430.
[17] N. Nithyadevi, P. Kandaswamy, Natural convection in a rectangular cavity with partially active side walls, Int. J. Heat and Mass Transfer 50, 4688-4697 (2007).